$FAPbI_3$ Perovskite Films Prepared by Solvent Self-volatilization for Photovoltaic Applications

Qiqi Zhang[a], Guorong Ma[b], Kevin A. Green[b], Kristine Gollinger[a], Jaiden Moore[a], Teresa Demeritte[a], Paresh Chandra Ray[a], Glake Alton Hill Jr[a], Xiaodan Gu[b], Sarah E. Morgan[b], Manliang Feng[c], Santanu Banerjee[c] and Qilin Dai[a]*

[a] *Department of Chemistry, Physics, and Atmospheric Sciences, Jackson State University, Jackson, MS, 39217, United States*

[b] *School of Polymer Science and Engineering, Center for Optoelectronic Materials and Devices, The University of Southern Mississippi, Hattiesburg, MS 39406, United States*

c *Department of Chemistry and Physics, Tougaloo College, Jacskon, MS, 39174, United States*

**Corresponding author: qilin.dai@jsums.edu*

Abstract:

Developing a simple method to synthesize the perovskite layer without the antisolvent technique can facilitate the industrial production of perovskite solar cells (PSCs). While limited progress has been made for the antisolvent-free method on formamidinium lead triiodide perovskite layers due to the phase stability issue. Here, we use N-methyl pyrrolidone (NMP) as an additive to inhibit the non-perovskite phase of $FAPbI_3$ to fabricate FAI-PbI_2-NMP intermediate phase via the self-volatilization of volatile solvent 2-methoxyethanol instead of the traditional anti-solvent method. The high-quality pure α phase of $FAPbI_3$ films is obtained by phase transition via annealing. The photovoltaic properties of the perovskite films affected by different NMP amounts are studied. The corresponding PSCs show a PCE of 20.1% compared to 15.6% for the PSCs fabricated with the classical antisolvent technique. The unencapsulated devices remain ~75% efficiency of their initial PCE values after 35 days of storage. This method can be used in scalable production of PSCs due to high reproducibility and easy operation.

Kewords: Antisolvent free method; Solvent volatilization; N-methyl pyrrolidone; 2-ME; Intermedia phase.

1. Introduction

Organic-inorganic hybrid perovskite solar cells (PSCs) have been investigated extensively in recent years.[1-3] The highest identified power conversion efficiency (PCE) of PSCs has been boosted to 25.5%.[4] The high efficiency is attributed to the excellent photoelectric properties of perovskite films, such as high absorption coefficient, long carrier diffusion length, and fast carrier mobility.[5-7] The perovskite films are dominated fabricated with the anti-solvent technique,[8-12] which cannot be utilized for large-area device production and the commercialization of PSCs. In addition, the anti-solvent method shows a very narrow processing window, which is not easy to control.[13-17] The time of ant-solvent dropping casting is very critical to the device performance.[18] Thus, antisolvent free methods were demonstrated, like spray coating method, inkjet printing, blade coating technique, and slot die coating,[19-25] but these methods are limited to the expensive and special equipment, not conducive to large-scale production and development for practical applications.

In recent years, the use of solvent self-volatilization during spin coating to form perovskite films has been developed.[26-29] In this method, The solvents with low boiling points and high vapor pressures can be removed quickly by self-volatilization during the high-speed spin coating process, leading to the formation of perovskite films. This method is believed to be a simple and efficient method. However, the nucleation rate is too fast in this method, leading to defect production in the perovskite films and low performance of the corresponding devices.[30-31] In order to obtain perovskite films with enhanced crystallization, improved surface coverage, and few defects, some researchers used additives or a second solvent to retard the crystallization process during the film formation. [19, 32-35] We developed an additive-based solvent self-volatilization during spin coating

using strong coordination additives in perovskite precursor solution to form the intermedia phase, then high-quality perovskite films can be achieved through the phase transition. We used methylammonium chloride (MACl) in the solution to form the MACl-PbI_2 intermedia phase via solvent self-volatilization in the process of spin coating to obtain high-quality perovskite films.[36] We also reported dimethyl sulfoxide (DMSO)-based methylammonium lead triiodide ($MAPbI_3$) intermediate phase fabrication by solvent self-volatilization during spin coating for PSCs.[37]

$MAPbI_3$ films have been investigated by the nonantisolvent method.[26, 28, 30] Formamidinium lead triiodide ($FAPbI_3$) exhibits a lower bandgap than $MAPbI_3$, which is much closer to Shockely-Queisser limit. Theoretically, $FAPbI_3$ can achieve higher efficiency than $MAPbI_3$. However, $FAPbI_3$ is easy to transform to non-photovoltaic phase at room temperature. The unwanted but more stable yellow δ-phase is very easy to form during the fabrication process. It is reported that pure phase $FAPbI_3$ was fabricated by blade-coating,[38] which is nonantisolvent method. However, the blade coating method requires special equipment, and the technique needs N_2 flow or heat as auxiliary means to facilitate solvent removal. Until now, it's still a challenge to prepare the high-efficiency FA-based perovskites by solvent self-volatilization without any auxiliary operations.

In this work, we successfully prepared high-quality $FAPbI_3$ perovskite films by solvent self-volatilization method through the FAI-PbI_2-NMP intermediate phase by spin coating. The improved film quality is attributed to the modulated nucleation and growth process of perovskite films caused by the FAI-PbI_2-NMP intermediate phase prepared via solvent self-volatilization in the process of spin coating. The best PCE of 20.1% is achieved for the corresponding PSCs. Such high efficiency suggests that the solvent self-volatilization method during spin coating is a facile and well-controlled technique for large area high-efficiency PSCs.

2. Experimental

2.1 Chemicals

Fluorine doped tin oxide (FTO) coated glasses were obtained from Advanced Election Technology CO,.Ltd. Zinc chloride, Titanium(IV) chloride , Gold wires, NMP were obtained from Alfa Aesar. MACl was provided by Xi'an Polymer Light Technology. Formamidinium iodide (FAI), 2-methoxyethanol (2-ME), DMSO, dimethylformamide (DMF), Chlorobenzene (CB), ACN, 2,2',7,7'-Tetrakis[N,N-di(4-methoxyphenyl)amino]-9,9'-spirobifluorene (Spiro-OMeTAD) were acquired from Sigma-Aldrich. PbI_2, Lithium bi(trifluoromethane) sulfonimide (Li-TFSI) were purchased from TCI. 4-tert-butylpyridine(4-tBP) was obtained from Accela.

2.2 Device fabrication

The FTO coated glass substrates were washed with deionized water, propanone, and isopropyl alcohol each with a ultrasound bath for 15 min each. Then the cleaned FTO substrates were treated by a heat gun to obtain dried substrates. Then followed by ultraviolet-ozone treatment for 30 min. An aqueous mixed $TiCl_4$ (0.2 M) and $ZnCl_2$ (0.009 M) solutions were prepared at 0 ºC. $ZnCl_2$ is used to reduce hysteresis of the devices according to the literature.[39] Compact TiO_2 layers on FTO glass were prepared by chemical bath deposition in the $TiCl_4$ solution at the temperature of 70 ºC for half an hour. Then, the coated substrates were cleaned by water and isopropanol. Afterward, The substrates were annealled at the temperature of 200 ºC for half an hour in ambient air. After that, the substrates were put into a nitrogen inert gas glove box to spin coat perovskite films. 1.33 M PbI_2, 1.33 M FAI and 1 ml 2-ME were mixed to prepare perovskite precursor. Then add 0.2 M MACl and different amount NMP (0%, 2.5%, 5%, 7.5%, 10% v/v) before spin coating. 30 µl perovskite solution was coated on the TiO_2 film at 8000 rpm for 30 s via spin coating. Then the perovskite films were moved to a hot plate annealing at 150 ºC for 10 mins. Spiro-MeOTAD (27

μL) was coated on the top of perovskite films with 4000 rpm for 30 s by spin coating. Then, the films were kept in a desiccator for 12 h. Au electrode with 60 nm thickness was coated on spiro-MeOTAD layer via a thermal evaporator with a shadow mask. 0.1 cm^2 device area is obtained by the masks. J-V curves were measured without any masks. For 10 cm *10 cm perovskite films, 1 ml perovskite precursor with 7.5% NMP was deposited on 10 cm * 10 cm FTO glass at 8000 rpm for 30 s by spin coating, then the perovskite films were transferred to a hot plate to anneal at 150 ^oC for 10 min.

2.3 Characterization and measurement

XRD experiments were carried out by a MiniFlex600 (Rigaku) with Cu Kα radiation (λ = 1.54056 Å). The UV-vis absorption spectra were recorded by a UV-vis spectrophotometer (Cary 60, Agilent Technologies). A field emission scanning electron microscope (LYR3 XMH, Tescan) was used to collect the scanning electron microscopy (SEM) data. The grazing-incidence wide-angle X-ray scattering (GIWAXS) diffraction patterns of the prepared perovskite films were studied with a laboratory beamline (Xenocs Inc. Xeuss 2.0), and the X-ray wavelength was 1.54 Å. The distance between the sample and the detector is 14.9 cm. The angle of 0.2^o was set for the measurement. The films were stored in a vacuum chamber to enhance the signal. Diffraction rings were collected with a Pilatus 1M detector from Dectris Inc. Dynamic light scattering (DLS) was performed on a Malvern Instruments Zetasizer Nano ZS (633 nm incident wavelength, 173° scattering angle) operating at 20 °C. The Fourier transform infrared spectra (FTIR) were measured by Spectrum Two FT-IR (PerkinElmer, USA). The current density-voltage curves were measured with a 2400 source meter from Keithley Instruments Inc. under the light irradiation from an AM 1.5G solar simulator (G2V Pico) with the light intensity of 100 mW cm^{-2}, which was confirmed with a Si cell from Newport (91150V). The incident photon-to-current efficiency (IPCE) data were

obtained with a IQE-200B (Newport). The photoluminescence (PL) data were collected by Horiba FluoroMAx fluorescence spectrometer. Time-resolved photoluminescence (TRPL) data were obtained by TCSPC technique through NanoLED and DeltaHub. 440 nm was used to pump the films to obtain PL spectra. A NanoLED (λ=451 nm) was used as light source to collect TRPL spectra. Impedance spectra of our devices were acquired with an CHI electrochemical workstation (604E) with a AC voltage of 5 mV, and the frequency was changed from 1 Hz to 1M Hz in the dark.

3. Results & discussion

The solvent self-volatilization method to prepare perovskite films is based on the fast volatilization of the solvent, leading to the quick nucleation and growth of perovskite grains and poor quality of the prepared perovskite films. In order to retard the nucleated rate, NMP has a strong interaction with both FAI and PbI_2 to form FAI-PbI_2-NMP structure in perovskite precursor, which could slow down the growth of perovskite grains, leading to high-quality perovskite films. NMP retards perovskite crystallization and improves the perovskite film quality.[40] If only minor coordinated solvents are used in our method, the perovskite films exhibit many pinholes, poor film coverage and small grain sizes due to too slow or too fast nucleation rates. These have been studied in our previous work.[36-37, 41] Therefore, the introduction of NMP can not create much more ionic defects in active layer. The perovskite precursor solution consists of FAI, PbI_2, and MACl, in the solvents of 2-ME and NMP. We tried MACl only to be used as an additive in this system. The film quality is too bad to fabricate devices. The solvent 2-ME is volatile solvents with very low boiling points and high vapor pressures, which is easy to realize volatilization, leading to wet perovskite film formation. In Figure 1, we prepare the wet films followed by thermal annealing to investigate

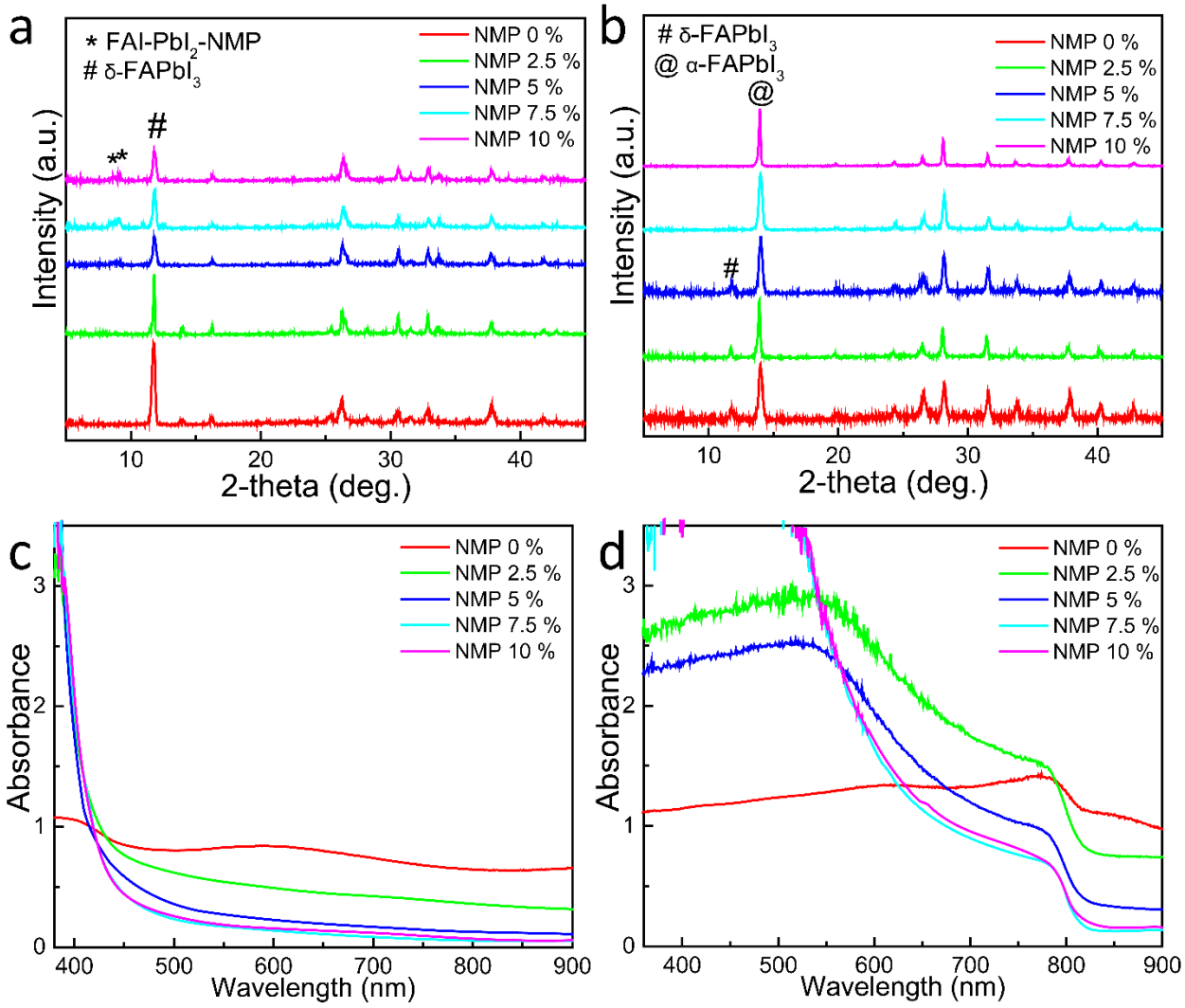

Figure 1. (a) the XRD patterns of the as-prepared wet films with various NMP concentrations (b) the XRD data of the annealed films (150 ◦C, 10 min). (c) UV–vis absorption spectra of the as prepared wet thin films prepared by different amounts of NMP. (d) UV–vis absorption of the annealed films after (150 ◦C , 10 min).

the phase transition. Figure 1a the XRD patterns of the as-prepared wet films with various NMP concentrations. Figure 1a shows that all the films contain the δ-phase $FAPbI_3$ with a diffraction peak at 11.8º. A peak at ~14º from α-phase is observed as NMP amounts are 0% and 2.5% v/v in perovskite precursor solution. When NMP amount increases to 5%, 7.5%, and 10%, the peak disappears, and the intermediate phase (labeled with *) is produced. This indicates that the

introduction of the NMP retards the growth of the α-phase. When NMP amount increases to 5%, 7.5%, and 10%, two tiny peaks at 8.56˚ and 9.07˚ appear. The XRD in Figure S1 indicates that the two peaks at 8.56˚ and 9.07˚ are attributed to FAI-PbI_2-NMP intermedia phase, which is consistent with the literature,[40] indicating the formation of the FAI-PbI_2-NMP intermedia phase by solvent self-volatilization during spin coating. After annealing the wet films at 150^o for 10 min, most δ-phase transfers to α-phase to form α/δ junction (Figure 1b). It can be observed that as the NMP content is less than 7.5%, the δ-phase $FAPbI_3$ still exists in the films, which are indicated by the tiny peaks at 11.8^o labeled by # in Figure 1b. However, all the δ-phase transfers to α-phase as the content of NMP is more than 7.5% (Figure. 1b). That means NMP could promote the phase transition from δ-phase to α-phase during the annealing in our method. The UV-vis absorption spectra of the wet films (before annealing) are shown in Figure 1c. No perovskite film absorption features are observed. 0% NMP film shows an absorption trend for perovskite film at 800 nm, but the typical perovskite absorption characteristics can not be observed for other curves contain the NMP. The film prepared without NMP shows a high baseline. The baselines decrease with the increase of NMP amount. An absorption edge at ~820 nm is observed for each film as the films are treated with annealing at the temperature 150 ^{o}C for 10 min shown in Figure 1d, indicating the formation of α-phase $FAPbI_3$. The films with NMP amount of 0%-5% exhibit a stage at ~350 nm -550 nm, which is attributed to the α/δ junction, and this is consistent with XRD results in Figure 1b. The tails (band gap) of the 2.5%, 5, and 7.5% films are different. This is explained by the difference film thickness, roughness, and the coverage of the films (Figure S2 and Figure 2). Therefore, the band gap estimated by UV-vis absorption spectra is not accurate due to the film thickness, roughness and coverage.

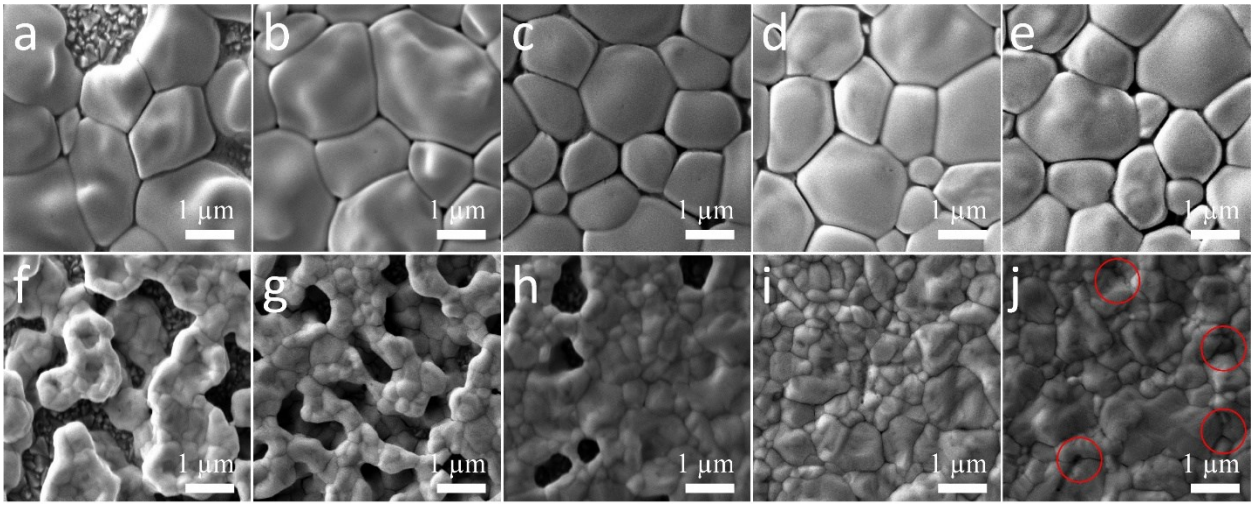

Figure 2. a-e the wet films prepared with 0%, 2.5%, 5%, 7.5%, 10% NMP. f-j the annealed perovskite films prepared by 0%, 2.5%, 5%, 7.5%, 10% amount NMP.

Figure 2 presents SEM data of the films fabricated with various NMP concentrations before and after thermal annealing to study the evolution of morphology and coverage of the films affected by annealing. Figure. 2a-e shows wet films prepared with different NMP amounts before annealing. The wet films with large grains exhibit uneven surfaces and pinholes. FTO glasses are observed from the pinholes of the perovskite films prepared without NMP (Figure 2a), indicating poor film coverage. The wet film with 0% NMP shows a mixture of both α and δ phase $FAPbI_3$. We can not observe the rod-like morphology for the yellow-$FAPbI_3$, which might be attributed to the addition of MACl or the films covarege that affects the yellow-$FAPbI_3$ growth process. Rod morphology yellow-$FAPbI_3$ was also not observed in Liu's work.[42] FTO glass can be fully covered by the wet films as NMP is added (Figure 2b-e). The amount of NMP doesn't affect the morphology of perovskite films in terms of grains sizes and FTO coverage. Figure 2f-j exhibits the SEM images of the annealed films (150 ºC, 10 min). Large grains composed of small particles are observed for the film prepared without NMP (Figure 2f). Therefore, the thermal treatment cannot enhance the coverage on the substartes for the film without NMP. When the NMP amount is 2.5% v/v (Figure

2g), the film still exhibits multi-layers and is composed of small particles. FTO glass substrate is fully covered, but the film shows many pinholes. The mean grain size grows from 200 to 800 nm when the NMP amount increases from 2.5% to 10% (Figure 2g-j). Figure 2i shows continuous and even film as the NMP amount is 7.5% v/v. The average grain size is about 600 nm. It can be observed 10% v/v NMP amount also leads to continuous film, but more pinholes are also observed which are labeled by red circles in Figure 2j. Figure S2 a-e shows that the cross-section SEM data of the perovskite films fabricated by various NMP concentrations. The thicknesses of perovskite films are 669 nm, 626 nm, 577 nm, 507 nm, and 500 nm for the thin films fabricated by the NMP amount of 0%, 2.5%, 5%, 7.5%, and 10%, respectively. The films show the mesoporous structure as the NMP amount is 0% and 2.5%. The dense and compact layer structure is observed as the NMP amount is 7.5% and 10%. Therefore, the film thickness decreases as the NMP amount increases. The films prepared with 7.5% v/v NMP show a uniform film structure. Therefore, NMP retards perovskite crystallization, and improves the perovskite grain quality. Excess NMP may accelerate the precursor solvation, which may lead to pinholes between the grains, which is detrimental to perovskite film fabrication for high-efficiency devices.[43]

Figure 3 shows growth mechanism of the perovskite films via the intermediate phase due to NMP. Figure 3a shows the schematic of the experimental procedures. First, we spin coat the perovskite precursor on TiO_2 surface. High-speed spin coating (8000 rpm) results in solvent volatilization to form wet films. Then the black perovskite phase is obtained by annealing on a hotplate. Figure 3b shows the status of FAI and PbI_2 dissolved in 2-ME solvent, indicating very weak interactions among them. The NMP is added to the solution to form FAI-PbI_2-NMP structures. The strong interactions among them benefit the production of high-quality perovskite

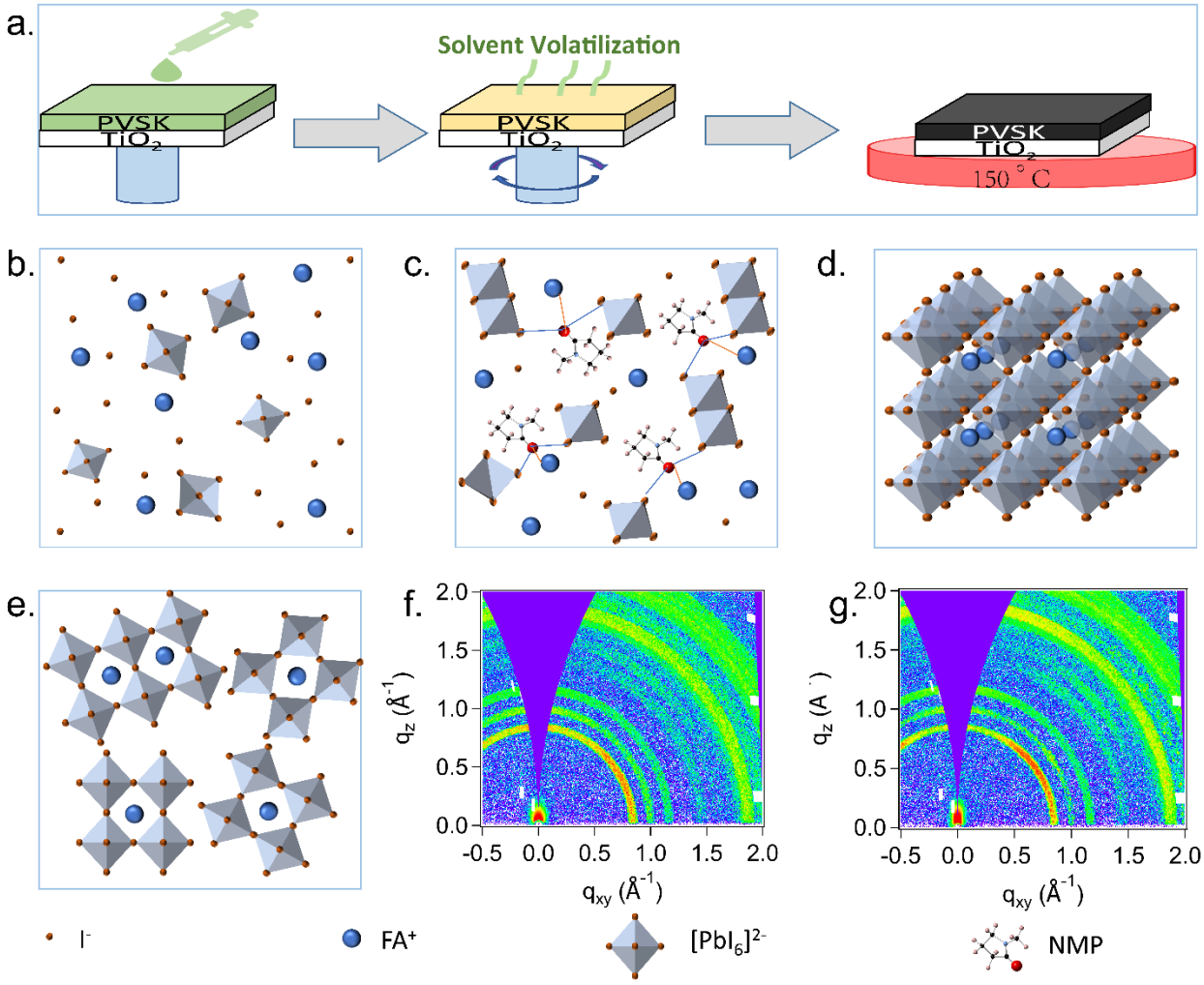

Figure 3. (a) the perovskite film synthesis method by our method. (b) FAI-PbI_2 prepared by dissolving PbI_2 and FAI in 2-ME. (c) FAI-PbI_2-NMP structures are formed due to the introduction of NMP. (d). Perovskite films with NMP after annealing. (e). perovskite film without NMP after annealing. (f). 2D GIWAXS patterns of perovskite films without NMP before annealing. (g). 2D GIWAXS pattern of perovskite with NMP before annealing.

films (Figure 3c). Figure S3 shows the size distribution of FAI-PbI_2 and FAI-PbI_2-NMP solutions studied by DLS, the peak around 5 nm can be assigned to Pb-I individual octahedrons, and the peak around 1000 nm can be assigned to the soft complex, which is consistent with literature.[44]

The Pb-I part occupies 59.83%, and soft complex part occupies 40.17% for the precusor without NMP.

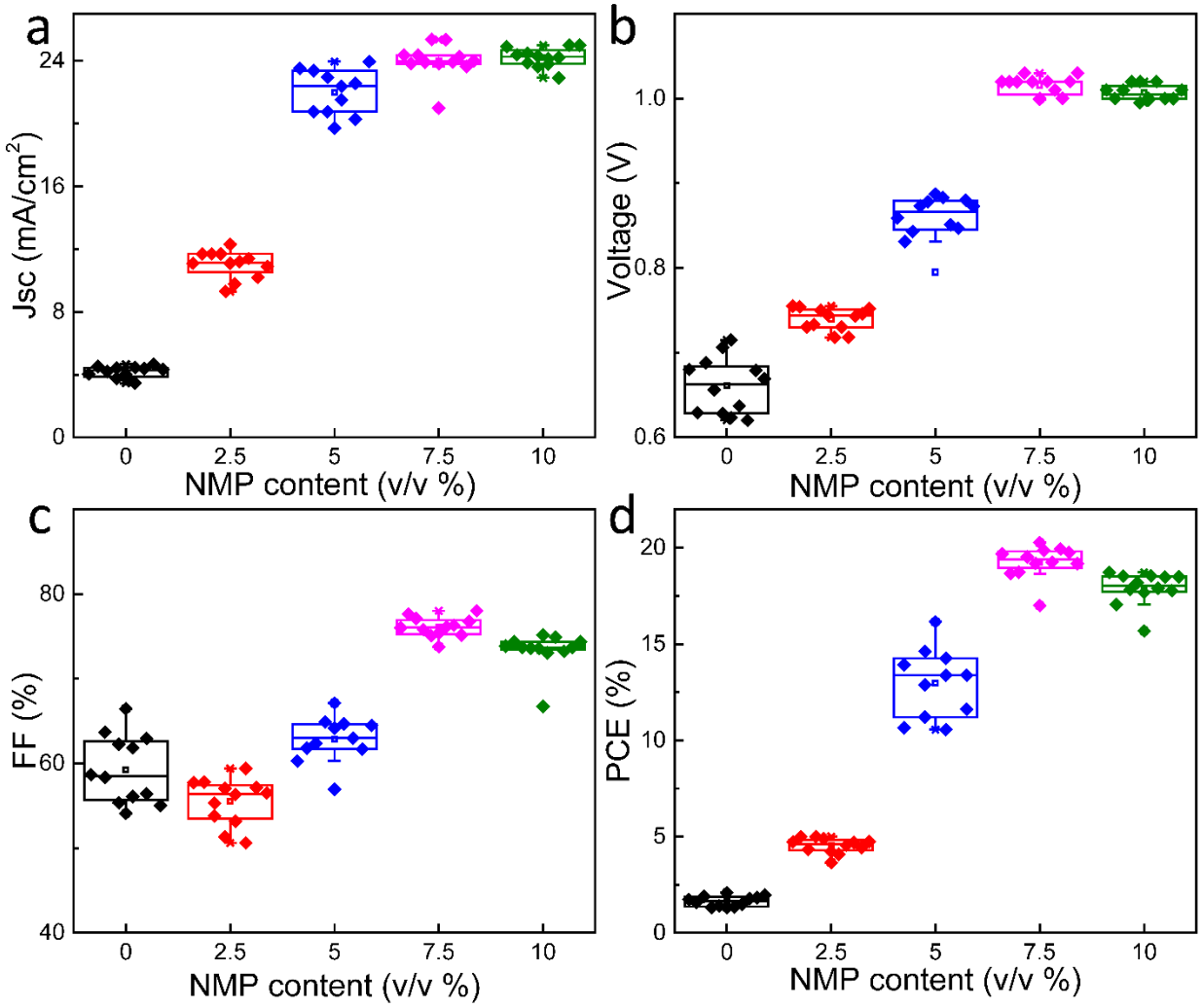

Figure 4. Statistics of photovoltaic parameters of PSCs with different amounts of NMP. (a). J_{sc}; (b) V_{oc}; (c) FF, (d) PCE.

The Pb-I part decrease to 31.7%, and the soft complx part increase to 68.3% for the precursor with 7.5% NMP. This indicates that NMP has a strong interaction with FAI and PbI_2.[40] Figure S4 shows the FTIR spectra of FAI in 2-ME, NMP solvent, perovskite solution without NMP and MACl and perovskite solution with 7.5% NMP and MACl. C=O bending vibration peak for NMP appears at

1685 cm^{-1}, and it shifts to 1633 cm^{-1} in PbI_2-NMP complex. The C=N bending vibration peak for FAI appears at 1697 cm^{-1}, and it shifts to 1708 cm^{-1} in FAI-PbI_2-NMP complex. These can be

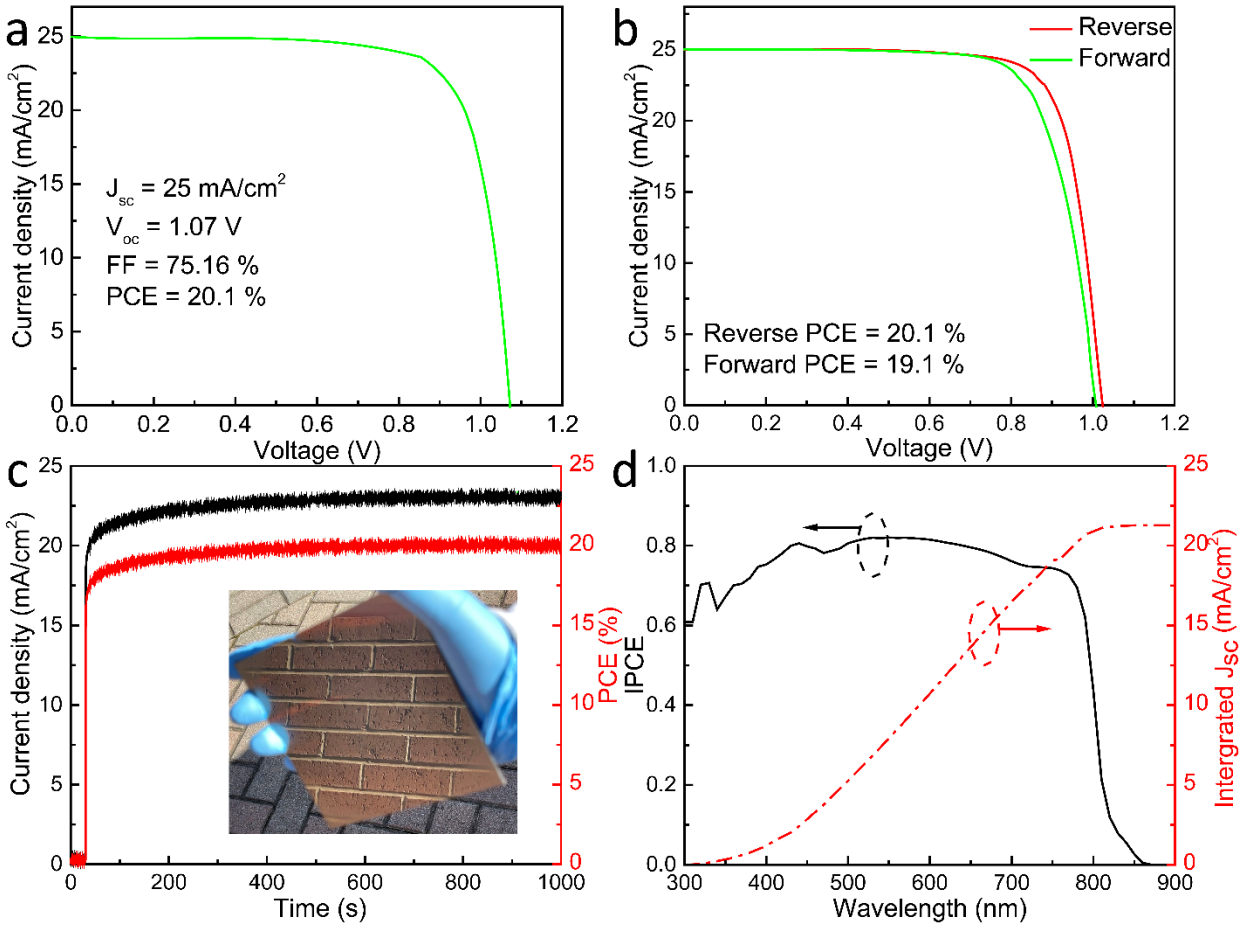

Figure 5. (a) the typical J-V data of the optimized device. (b) J-V curve of a typical PSC based on 7.5% NMP at the reverse and forward scan directions. (c). stabilized power output for best devices. The inset one is the photograph of one large area perovskite film with a size of 10 cm * 10 cm. (d) IPCE for optimal devices.

explained by the strong interaction between NMP, FAI and PbI_2 according to the literature.[40] After annealing, pure α phase perovskite films are formed (Figure 3d) due to the retarded growth process of perovskite grains caused by NMP. As for the films without NMP, a disordered perovskite structure is obtained due to the fast perovskite growth caused by the fast nucleation process (Figure

3e). No intermedia phase is obtained for the film prepared without NMP, which is confirmed by XRD results in Figure 1a. Figures 3 f and g show the 2D GIWAXS diffraction patterns of the perovskite films prepared without and with NMP, respectively. The scattering ring (q=1 $Å^{-1}$) is attributed to (001) crystal plane for perovskite films.[45] No additional rings from the intermediate phase are observed from the 2D GIWAXS data of the NMP-based perovskite films , which is attributed to the crystal phase transition from intermediate phase to normal perovskite phase during the shipping and handling.

The photovoltaic parameters of the PSCs with different NMP amounts are shown in Figure 4. The short-circuit current (J_{sc}) increases with the increase of NMP. J_{sc} of the PSCs with 5-10% NMP is almost 5 times as large as the PSCs without NMP. Figure 4b shows the open-circuit voltage (V_{oc}) also increases substantially as NMP is introduced to the films. In Figure 4c, the fill factor (FF) values increase from 56% to 75% as the NMP amounts increase from 0% to 7.5%. PSCs with 10% NMP show an FF of 70% which is smaller than that of the PSCs with 7.5% NMP, which is explained by the pinholes of the 10% NMP films (Figure 2j). 7.5% NMP devices exhibit the highest PCE. The low PCE of the devices based on 0%, 2.5%, and 5% compared to the NMP 7.5% is also associate with the excessive thickness of the film. The films prepared with 7.5% and 10% NMP show the similar thicknesses, and the lower PCE of the device with 10% NMP is attributed to the film morphology and film quality. Therefore, the optimal NMP concentration is 7.5%. Figure 5a shows the typical J-V data of the optimized device. The values of J_{sc}, V_{oc}, and FF are 25 mA/cm^2, 1.07 V, and 75.16%, respectively, yielding 20.1% efficiency. Antisolvent method based on CB was used to fabricate perovskite films (Figure S5), and the perovskite solution was prepared by DMF and DMSO (4:1, V/V). The device shows a efficiency of 15.6% for reverse scan direction, and the forward scan produces a PCE of 15.6%. We optimized the fabrication procedure of the

traditional antisolvent method, and a PCE of 15.6% is obtained. However, this can not be used to show the traditional antisolvent method is not as good as our method. Our

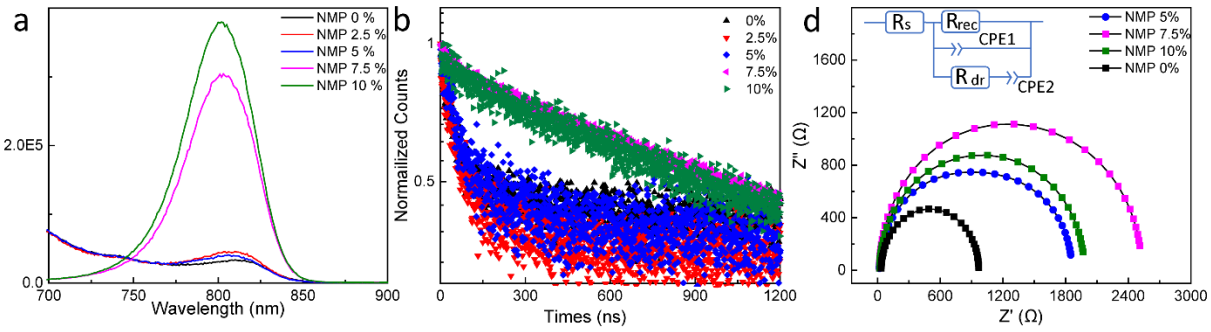

c

	τ₁ (ns)	A₁ (%)	τ₂ (ns)	A₂ (%)
NMP 0 %	17.14	34.3	110.8	65.7
NMP 2.5 %	22.25	36.16	168.9	63.84
NMP 5 %	23.3	34.93	162.7	65.07
NMP 7.5 %	52.16	2.61	811.52	97.39
NMP 10 %	92.08	2.13	639.34	97.87

Figure 6. (a) the PL data of the perovskite films with various NMP concentrations. (b) the TRPL data of (a) films; (c) the fitting parameters obtained by bi-exponential equation for TRPL data. (d) the impedance spectra of PSCs with different amounts of NMP.

method is very promising in high-performance PSCs. Figure. 5b shows that the device efficiencies are 20.06% and 19.1% obtained by reverse and forward scans, respectively, indicating the smaller hysteresis effects in our perovskite films due to few defects. The stable PCE of 20% is obtained when 0.87 V is applied to the device, showing good light stability (Figure 5c). The perovskite film with a large area of 10 cm* 10 cm is shown inset of Figure 5c, It's a mirror-like perovskite film, and it shows a wall. The video S1 shows the the film formation, which exhibits the feasibility of the developed method in practical applications for large area devices. The device stability is shown in Figure S6. The unencapsulated device is maintained in the air for 35 days with a RH of ~ 20%. The PCE values of 0%-5% NMP-based PSCs decrease 20% of their initial values within 20 days,

but the PCE of 7.5% and 10% NMP-based PSCs drops to ~75% of the original PCE after 35 days, which shows device good stability as 7.5% and 10% NMP is used for device fabrication. Figure 5d shows the IPCE spectrum of the optimized PSC. The intensity of IPCE reaches 80% in 450 – 650 nm. The calculated J_{sc} is 21.3 mA/cm^2 by integrating, and the J_{sc} from J-V curve is 25 mA/cm^2. It is believed that the integrated current density obtained from IPCE is less than Jsc from J−V curves within 10-20% is reasonable. The reason for the difference is attributed to the light source, ion migration, and degradation of the perovskite films under long time light irradiation during IPCE measurements.[46] In addition, external bias leads to ion movement inside the perovskite films, which is another reason for the low integrated J_{sc}.[46] Moreover, IPCE results are also dependent on the frequency of the measurement.[46]

The optical properties of the films with different NMP amounts are studied by PL and TRPL techniques to understand the improved device performance caused by NMP. All the films are deposited on the glass substrate. Figure 6a shows the PL spectra of the film prepared with different NMP amounts. It can be observed that the peak positions locate at ~800 nm. The PL peak positions of the films exhibit blueshift as the NMP amount increases, indicating that NMP effectively passivates the defects in perovskite films according to the literature.[47-48] The films with 0%, 2.5%, and 5% NMP show low PL intensity compared to the films with 7.5% and 10% NMP, which is attributed to the discontinuous film properties (Figure 2 f-h). Therefore, it is hard to compare the PL intensities of for these three films (0%, 2.5%, and 5%). The films with 7.5% and 10% NMP show much higher intensities compared to the films with 0%, 2.5%, and 5% NMP due to the improved film quality caused by NMP (Figure 2 i and j). The TRPL data of films prepared with various NMP concentrations are shown in Figure 6b. The TRPL curves are fitted by the bi-

exponential decay function and the fitting parameters are shown in Figure 6c, the equation shows below,

$$Y = A_1 \exp\left(\frac{-t}{\tau_1}\right) + A_2 \exp\left(\frac{-t}{\tau_2}\right)$$

Where A1 and A2 are the relative amplitudes; τ1 and τ2 are the values of the lifetime for the fast and slow decay, respectively. The fast decay is associated to trap-assisted non-radiative recombination at the film surface,[49-50] and the slow decay is attributed to the radiative recombination in GBs of the perovskite films. [50-51] TRPL data in Figure 6b and c show that the lifetims of the films with 0%, 2.5%, and 5% are very similar to each other. The lifetimes of the films with 7.5% and 10% NMP exhibt longer lifetime than that of the films prepared with 0%, 2.5%, and 5% NMP, which is explained by the reduced defects by NMP. Figure S7 shows J-V curves of electron-only (FTO/TiO_2/PVSK/PCBM/Au) and hole-only devices (FTO/PTAA/PVSK/Spiro/Au). The linear-relationship region represents an ohmic response at low voltage, and the kink point is trap-filled limit voltage (V_{TFL}). Considering a linear dependence between trap density (ηtraps) and V_{TFL}, the ηtraps can be calculated by the follow equation,

$$\eta_{traps} = \frac{2\varepsilon\varepsilon_0 V_{TFL}}{eL^2}$$

Where e is the elementary charge of an electron; ε and ε0 are the relative dielectric constant of $FAPbI_3$ and vacuum dielectric constant, respectively, and L is the thickness of the perovskite layer. The calculated electron-trap density values of PSCs with and without NMP are $1.296*10^{17}$ cm^{-3} and $1.324*10^{17}$ cm^{-3}, respectively. The hole-trap density values of PSCs with and without NMP are $5.77*10^{17}$ cm^{-3} and $6.41*10^{17}$ cm^{-3}. These results indicate NMP modification reduces electron and hole -trap densities of the films. Figure 6d shows the Nyquist plot of the PSCs based on

different NMP amounts (0%, 5%, 7.5%, and 10%). The R_s is the series resistance related to FTO. R_{rec} represents the recombination resistance of the devices, CPE1 is the contact capacitance that is derived from charge buildup at the interfaces between the perovskite film and its adjacent contacts, R_{dr} is the dielectric relaxation resistance, CPE2 is the capacitance of the perovskite films. The EIS data can be well fitted with the circuit shown in the inset of Figure 6d, and the results are shown in Table S1. Compared to the R_{rec} of 0%, 5% and 10% NMP devices (998 Ω, 1842 Ω and 1959 Ω), the device with 7.5% NMP shows a larger R_{rec} (2511 Ω), which confirms that the charge recombination loss is suppressed for the 7.5% NMP device.

4. Conclusions

We demonstrate a facile method to fabricate $FAPbI_3$ films with high quality by solvent self-volatilization. The intermediate phase of FAI-PbI_2-NMP films is fabricated via solvent self-volatilization in the process of spin coating. High-quality photovoltaic phase $FAPbI_3$ films are obtained by annealing the intermedia phase via controlling the amount of NMP. The PSCs based on the prepared $FAPbI_3$ films are fabricated and studied. The PSCs show high reproducibility and high efficiency toward practical applications. The best PCE of 20.1 % is achieved compared to 15.6% by the traditional antisolvent method. This work also shows the feasibility to prepare large-scale production and large area devices of PSCs for practical applications.

Supporting Information

XRD patterns of FAI-PbI_2-NMP and FAI-PbI_2-MACl spin-coated films. Cross-section for different amount NMP prepared perovskite solar cells. (a). 0% NMP; (b). 2.5% NMP; (c). 5% NMP; (d). 7.5% NMP; (e). 10% NMP. DLS profiles of precursor solutions of FAI-PbI_2 and FAI-PbI_2-NMP in 2ME. FTIR spectra for FAI and in 2ME; NMP solvent; perovskite solution without NMP and MACl and

perovskite solution with 7.5% NMP and MACl. The J-V data of PSC fabricated with antisolvent technique measured through the reverse and forward scans. The device aging stability for different amount NMP perovskite solar cell. Current-voltage curves of electron-only device (a) and hole-only (b) device based on 0% and 7.5% NMP perovskites.

Author Information

Corresponding Author

Qilin Dai: Department of Chemistry, Physics, and Atmospheric Sciences, Jackson State University, Jackson, Mississippi, 39217, United States.

Email: qilin.dai@jsums.edu

Authors

Qiqi Zhang: Department of Chemistry, Physics, and Atmospheric Sciences, Jackson State University, Jackson, MS, 39217, United States

Guorong Ma: School of Polymer Science and Engineering, Center for Optoelectronic Materials and Devices, The University of Southern Mississippi, Hattiesburg, MS 39406, United States

Kevin A. Green: School of Polymer Science and Engineering, Center for Optoelectronic Materials and Devices, The University of Southern Mississippi, Hattiesburg, MS 39406, United States

Kristine Gollinger: Department of Chemistry, Physics, and Atmospheric Sciences, Jackson State University, Jackson, MS, 39217, United States

Jaiden Moore: Department of Chemistry, Physics, and Atmospheric Sciences, Jackson State University, Jackson, MS, 39217, United States

Teresa Demeritte: Department of Chemistry, Physics, and Atmospheric Sciences, Jackson State University, Jackson, MS, 39217, United States

Paresh Chandra Ray: Department of Chemistry, Physics, and Atmospheric Sciences, Jackson State University, Jackson, MS, 39217, United States

Glake Alton Hill Jr: Department of Chemistry, Physics, and Atmospheric Sciences, Jackson State University, Jackson, MS, 39217, United States

Xiaodan Gu: School of Polymer Science and Engineering, Center for Optoelectronic Materials and Devices, The University of Southern Mississippi, Hattiesburg, MS 39406, United States

Sarah E. Morgan: School of Polymer Science and Engineering, Center for Optoelectronic Materials and Devices, The University of Southern Mississippi, Hattiesburg, MS 39406, United States

Manliang Feng: Department of Chemistry and Physics, Tougaloo College, Jacskon, MS, 39174, United States

Santanu Banerjee: Department of Chemistry and Physics, Tougaloo College, Jacskon, MS, 39174, United States

Author Contributions

Qiqi Zhang carried out the experiments and wrote the draft of the manuscript. Guorong Ma and Xiaodan Gu collected the 2D GIWAXS diffraction patterns. synthesized the NIR dyes. Kevin A. Green, Sarah E. Morgan, Manliang Feng, and Santanu Banerjee carried out the DLS measurements.

Kristine Gollinger, Jaiden Moore, Teresa Demeritte, Paresh Chandra Ray and Glake Alton Hill Jr helped with the understanding of the perovskite film growth by discussion. Qilin Dai supervised the project. All authors have approved the final version of the manuscript.

Notes

The authors declare no competing financial interest.

ACKNOWLEDGMENT

This work is supported by NSF-PREM grant #DMR-1826886. The steady-state PL and TRPL equipment used in this work is supported by National Science Foundation Research Initiation Award: Novel Perovskite Solar Cells Based on Interface Manipulation (Award#1900047). G. M. and X.G. thank NSF grant OIA- 1757220 for providing financial support. Jaiden Moore is supported by 2020 MS NASA EPSCOR RID SEED GRANTS 361559 (G00005391).

References

(1) Kim, G.; Min, H.; Lee, K. S.; Yoon, S. M.; Seok, S. I. Impact of strain relaxation on performance of α-formamidinium lead iodide perovskite solar cells. *Science* **2020,** *370* (6512), 108-112.
(2) Kojima, A.; Teshima, K.; Shirai, Y.; Miyasaka, T. Organometal halide perovskites as visible-light sensitizers for photovoltaic cells. *J. Am. Chem.Soc.* **2009,** *131* (17), 6050-6051.
(3) Jeong, J.; Kim, M.; Seo, J.; Lu, H.; Ahlawat, P.; Mishra, A.; Yang, Y.; Hope, M. A.; Eickemeyer, F. T.; Kim, M. Pseudo-halide anion engineering for α-$FAPbI_3$ perovskite solar cells. *Nature* **2021,** *592* (7854), 381-385.
(4) Yoo, J. J.; Seo, G.; Chua, M. R.; Park, T. G.; Lu, Y.; Rotermund, F.; Kim, Y.-K.; Moon, C. S.; Jeon, N. J.; Correa-Baena, J.-P. Efficient perovskite solar cells via improved carrier management. *Nature* **2021,** *590* (7847), 587-593.
(5) Xing, G.; Mathews, N.; Sun, S.; Lim, S. S.; Lam, Y. M.; Grätzel, M.; Mhaisalkar, S.; Sum, T. C. Long-range balanced electron-and hole-transport lengths in organic-inorganic $CH_3NH_3PbI_3$. *Science* **2013,** *342* (6156), 344-347.
(6) Stranks, S. D.; Eperon, G. E.; Grancini, G.; Menelaou, C.; Alcocer, M. J.; Leijtens, T.; Herz, L. M.; Petrozza, A.; Snaith, H. J. Electron-hole diffusion lengths exceeding 1 micrometer in an organometal trihalide perovskite absorber. *Science* **2013,** *342* (6156), 341-344.
(7) Hao, F.; Stoumpos, C. C.; Cao, D. H.; Chang, R. P.; Kanatzidis, M. G. Lead-free solid-state organic–inorganic halide perovskite solar cells. *Nat. photonics* **2014,** *8* (6), 489-494.

(8) Dong, C.; Han, X.; Zhao, Y.; Li, J.; Chang, L.; Zhao, W. A green anti-solvent process for high performance carbon-based $CsPbI_2Br$ all-inorganic perovskite solar cell. *Sol. RRL* **2018,** *2* (9), 1800139.
(9) Konstantakou, M.; Perganti, D.; Falaras, P.; Stergiopoulos, T. Anti-solvent crystallization strategies for highly efficient perovskite solar cells. *Crystals* **2017,** *7* (10), 291.
(10) Tavakoli, M. M.; Yadav, P.; Prochowicz, D.; Sponseller, M.; Osherov, A.; Bulović, V.; Kong, J. Controllable perovskite crystallization via antisolvent technique using chloride additives for highly efficient planar perovskite solar cells. *Adv. Energy Mater.* **2019,** *9* (17), 1803587.
(11) Jeon, N. J.; Noh, J. H.; Yang, W. S.; Kim, Y. C.; Ryu, S.; Seo, J.; Seok, S. I. Compositional engineering of perovskite materials for high-performance solar cells. *Nature* **2015,** *517* (7535), 476-480.
(12) Cho, K. T.; Paek, S.; Grancini, G.; Roldán-Carmona, C.; Gao, P.; Lee, Y.; Nazeeruddin, M. K. Highly efficient perovskite solar cells with a compositionally engineered perovskite/hole transporting material interface. *Energy Environ. Sci.* **2017,** *10* (2), 621-627.
(13) Zheng, X.; Chen, B.; Wu, C.; Priya, S. Room temperature fabrication of $CH_3NH_3PbBr_3$ by anti-solvent assisted crystallization approach for perovskite solar cells with fast response and small J–V hysteresis. *Nano Energy* **2015,** *17*, 269-278.
(14) Zhang, M.; Wang, Z.; Zhou, B.; Jia, X.; Ma, Q.; Yuan, N.; Zheng, X.; Ding, J.; Zhang, W. H. Green Anti-Solvent Processed Planar Perovskite Solar Cells with Efficiency Beyond 19%. *Sol. RRl* **2018,** *2* (2), 1700213.
(15) Jin, S.; Wei, Y.; Huang, F.; Yang, X.; Luo, D.; Fang, Y.; Zhao, Y.; Guo, Q.; Huang, Y.; Wu, J. Enhancing the perovskite solar cell performance by the treatment with mixed anti-solvent. *J. Power Sources* **2018,** *404*, 64-72.
(16) Jeon, N. J.; Noh, J. H.; Kim, Y. C.; Yang, W. S.; Ryu, S.; Seok, S. I. Solvent engineering for high-performance inorganic–organic hybrid perovskite solar cells. *Nat. Mater.* **2014,** *13* (9), 897-903.
(17) Ahn, N.; Son, D.-Y.; Jang, I.-H.; Kang, S. M.; Choi, M.; Park, N.-G. Highly reproducible perovskite solar cells with average efficiency of 18.3% and best efficiency of 19.7% fabricated via Lewis base adduct of lead (II) iodide. *J. Am. Chem.Soc.* **2015,** *137* (27), 8696-8699.
(18) Hamill Jr, J. C.; Schwartz, J.; Loo, Y.-L. Influence of solvent coordination on hybrid organic–inorganic perovskite formation. *ACS Energy Lett.* **2017,** *3* (1), 92-97.
(19) Zhang, J.; Bu, T.; Li, J.; Li, H.; Mo, Y.; Wu, Z.; Liu, Y.; Zhang, X.-L.; Cheng, Y.-B.; Huang, F. Two-step sequential blade-coating of high quality perovskite layers for efficient solar cells and modules. *J. Mater. Chem. A* **2020,** *8* (17), 8447-8454.
(20) Yang, Z.; Zhang, W.; Wu, S.; Zhu, H.; Liu, Z.; Liu, Z.; Jiang, Z.; Chen, R.; Zhou, J.; Lu, Q. Slot-die coating large-area formamidinium-cesium perovskite film for efficient and stable parallel solar module. *Sci. Adv.* **2021,** *7* (18), eabg3749.
(21) Deng, Y.; Zheng, X.; Bai, Y.; Wang, Q.; Zhao, J.; Huang, J. Surfactant-controlled ink drying enables high-speed deposition of perovskite films for efficient photovoltaic modules. *Nat. Energy* **2018,** *3* (7), 560-566.
(22) Bishop, J. E.; Mohamad, D. K.; Wong-Stringer, M.; Smith, A.; Lidzey, D. G. Spray-cast multilayer perovskite solar cells with an active-area of 1.5 cm^2. *Sci. Rep.* **2017,** *7* (1), 1-11.
(23) Wei, Z.; Chen, H.; Yan, K.; Yang, S. Inkjet printing and instant chemical transformation of a $CH_3NH_3PbI_3$/nanocarbon electrode and interface for planar perovskite solar cells. *Angew. Chem.* **2014,** *126* (48), 13455-13459.
(24) Li, Z.; Li, P.; Chen, G.; Cheng, Y.; Pi, X.; Yu, X.; Yang, D.; Han, L.; Zhang, Y.; Song, Y. Ink engineering of inkjet printing perovskite. *ACS Appl. Mater. Interfaces* **2020,** *12* (35), 39082-39091.
(25) Li, P.; Liang, C.; Bao, B.; Li, Y.; Hu, X.; Wang, Y.; Zhang, Y.; Li, F.; Shao, G.; Song, Y. Inkjet manipulated homogeneous large size perovskite grains for efficient and large-area perovskite solar cells. *Nano Energy* **2018,** *46*, 203-211.
(26) Deng, Y.; Van Brackle, C. H.; Dai, X.; Zhao, J.; Chen, B.; Huang, J. Tailoring solvent coordination for high-speed, room-temperature blading of perovskite photovoltaic films. *Sci. Adv.* **2019,** *5* (12), eaax7537.

(27) Lee, J.-W.; Na, S.-I.; Kim, S.-S. Efficient spin-coating-free planar heterojunction perovskite solar cells fabricated with successive brush-painting. *J. Power Sources* **2017,** *339*, 33-40.
(28) Li, J.; Dagar, J.; Shargaieva, O.; Flatken, M. A.; Köbler, H.; Fenske, M.; Schultz, C.; Stegemann, B.; Just, J.; Többens, D. M. 20.8% Slot-Die Coated $MAPbI_3$ Perovskite Solar Cells by Optimal DMSO-Content and Age of 2-ME Based Precursor Inks. *Adv. Energy Mater.* **2021,** *11* (10), 2003460.
(29) Yang, Z.; Liu, Z.; Ahmadi, V.; Chen, W.; Qi, Y. Recent Progress on Metal Halide Perovskite Solar Minimodules. *Sol. RRL* **2021**, 2100458.
(30) Wang, G.; Liao, L.; Chen, L.; Xu, C.; Yao, Y.; Liu, D.; Li, P.; Deng, J.; Song, Q. Perovskite solar cells fabricated under ambient air at room temperature without any post-treatment. *Org. Electron.* **2020,** *86*, 105918.
(31) Hendriks, K. H.; van Franeker, J. J.; Bruijnaers, B. J.; Anta, J. A.; Wienk, M. M.; Janssen, R. A. 2-Methoxyethanol as a new solvent for processing methylammonium lead halide perovskite solar cells. *J. Mater. Chem. A* **2017,** *5* (5), 2346-2354.
(32) Du, M.; Zhu, X.; Wang, L.; Wang, H.; Feng, J.; Jiang, X.; Cao, Y.; Sun, Y.; Duan, L.; Jiao, Y. High-Pressure Nitrogen-Extraction and Effective Passivation to Attain Highest Large-Area Perovskite Solar Module Efficiency. *Adv. Mater.* **2020,** *32* (47), 2004979.
(33) Chu, S.; Chen, W.; Fang, Z.; Xiao, X.; Liu, Y.; Chen, J.; Huang, J.; Xiao, Z. Large-area and efficient perovskite light-emitting diodes via low-temperature blade-coating. *Nat. Commun.* **2021,** *12* (1), 1-9.
(34) Chen, C.-L.; Zhang, S.-S.; Liu, T.-L.; Wu, S.-H.; Yang, Z.-C.; Chen, W.-T.; Chen, R.; Chen, W. Improved open-circuit voltage and ambient stability of $CsPbI_2Br$ perovskite solar cells by incorporating CH_3NH_3Cl. *Rare Met.* **2020,** *39* (2), 131-138.
(35) Kim, M.; Kim, G.; Lee, T.; Choi, I.; Choi, H.; Jo, Y.; Yoon, Y.; Kim, J.; Lee, J.; Huh, D., Methylammonium Chloride Induces Intermediate Phase Stabilization for Efficient Perovskite Solar Cells, *Joule*. 3 (2019) 2179–2192.
(36) Li, B.; Zhang, Q.; Zhang, S.; Ahmad, Z.; Chidanguro, T.; Davis, A. H.; Simon, Y. C.; Gu, X.; Zheng, W.; Pradhan, N. Spontaneously supersaturated nucleation strategy for high reproducible and efficient perovskite solar cells. *Chem. Eng. J.* **2021,** *405*, 126998.
(37) Zhang, Q.; Qi, Y.; Conkle, K.; Xiong, J.; Box, D.; Ray, P.; Pradhan, N. R.; Shahbazyan, T. V.; Dai, Q. Perovskite films prepared by solvent volatilization via DMSO-based intermediate phase for photovoltaics. *Sol. Energy* **2021,** *218*, 383-391.
(38) Yang, F.; Dong, L.; Jang, D.; Tam, K. C.; Zhang, K.; Li, N.; Guo, F.; Li, C.; Arrive, C.; Bertrand, M. Fully Solution Processed Pure α-Phase Formamidinium Lead Iodide Perovskite Solar Cells for Scalable Production in Ambient Condition. *Adv. Energy Mate.* **2020,** *10* (42), 2001869.
(39) Liu, X.; Wu, Z.; Zhang, Y.; Tsamis, C. Low temperature Zn-doped TiO_2 as electron transport layer for 19% efficient planar perovskite solar cells. *Appl. Surf. Sci.* **2019,** *471*, 28-35.
(40) Wu, C.; Wang, D.; Zhang, Y.; Gu, F.; Liu, G.; Zhu, N.; Luo, W.; Han, D.; Guo, X.; Qu, B. $FAPbI_3$ flexible solar cells with a record efficiency of 19.38% fabricated in air via ligand and additive synergetic process. *Adv. Funct. Mater.* **2019,** *29* (34), 1902974.
(41) Zhang, Q.; Conkle, K.; Ahmad, Z.; Ray, P. C.; Kołodziejczyk, W.; Hill, G. A.; Gu, X.; Dai, Q. $(FA_{0.83}MA_{0.17})_{0.95}Cs_{0.05}Pb(I_{0.83}Br_{0.17})_3$ Perovskite Films Prepared by Solvent Volatilization for High-Efficiency Solar Cells. *Sol. RRL* **2021,** *5* (11), 2100640.
(42) Deng, W.; Li, F.; Li, J.; Wang, M.; Hu, Y.; Liu, M. Anti-solvent free fabrication of FA-Based perovskite at low temperature towards to high performance flexible perovskite solar cells. *Nano Energy* **2020,** *70*, 104505.
(43) Zhu, J.; Park, S.; Gong, O. Y.; Sohn, C.; Li, Z.; Zhang, Z.; Jo, B.; Kim, W.; Han, G. S.; Kim, D. H. Formamidine disulfide oxidant as a localised electron scavenger for> 20% perovskite solar cell modules. *Energy Environ. Sci.* **2021,** 4903-4914.

(44) Xie, L.; Lin, K.; Lu, J.; Feng, W.; Song, P.; Yan, C.; Liu, K.; Shen, L.; Tian, C.; Wei, Z. Efficient and stable low-bandgap perovskite solar cells enabled by a $CsPbBr_3$-cluster assisted bottom-up crystallization approach. *J. Am. Chem.Soc.* **2019,** *141* (51), 20537-20546.
(45) Liu, Y.; Akin, S.; Hinderhofer, A.; Eickemeyer, F. T.; Zhu, H.; Seo, J. Y.; Zhang, J.; Schreiber, F.; Zhang, H.; Zakeeruddin, S. M. Stabilization of highly efficient and stable phase-pure $FAPbI_3$ perovskite solar cells by molecularly tailored 2D-overlayers. *Angew. Chem. Int. Ed.* **2020,** *59* (36), 15688-15694.
(46) Saliba, M.; Etgar, L. Current density mismatch in perovskite solar cells. *ACS Energy Lett.* **2020,** *5* (9), 2886-2888.
(47) Li, H.; Bu, T.; Li, J.; Lin, Z.; Pan, J.; Li, Q.; Zhang, X.-L.; Ku, Z.; Cheng, Y.-B.; Huang, F. Ink Engineering for Blade Coating FA-Dominated Perovskites in Ambient Air for Efficient Solar Cells and Modules. *ACS Appl. Mater. Interfaces* **2021,** *13* (16), 18724-18732.
(48) Wu, W. Q.; Rudd, P. N.; Wang, Q.; Yang, Z.; Huang, J. Blading Phase-Pure Formamidinium-Alloyed Perovskites for High-Efficiency Solar Cells with Low Photovoltage Deficit and Improved Stability. *Adv. mater.* **2020,** *32* (28), 2000995.
(49) Liu, B.; Bi, H.; He, D.; Bai, L.; Wang, W.; Yuan, H.; Song, Q.; Su, P.; Zang, Z.; Zhou, T. Interfacial Defect Passivation and Stress Release via Multi-Active-Site Ligand Anchoring Enables Efficient and Stable Methylammonium-Free Perovskite Solar Cells. *ACS Energy Lett.* **2021,** *6*, 2526-2538.
(50) Guo, P.; Ye, Q.; Yang, X.; Zhang, J.; Xu, F.; Shchukin, D.; Wei, B.; Wang, H. Surface & grain boundary co-passivation by fluorocarbon based bifunctional molecules for perovskite solar cells with efficiency over 21%. *J. Mater. Chem. A* **2019,** *7* (6), 2497-2506.
(51) Handa, T.; Tex, D. M.; Shimazaki, A.; Wakamiya, A.; Kanemitsu, Y. Charge injection mechanism at heterointerfaces in $CH_3NH_3PbI_3$ perovskite solar cells revealed by simultaneous time-resolved photoluminescence and photocurrent measurements. *J. Phys. Chem. Lett.* **2017,** *8* (5), 954-960.

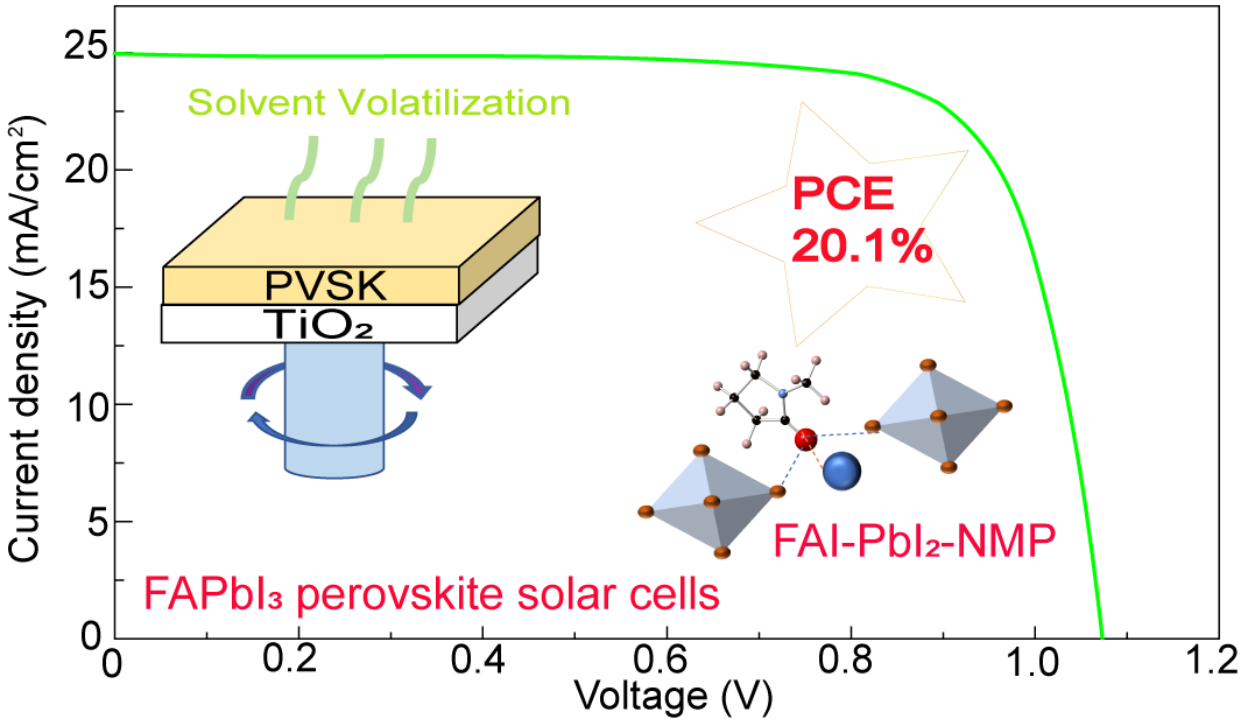
Solvent Volatilization
PVSK
TiO2
PCE
20.1%
FAI-PbI2-NMP
FAPbI3 perovskite solar cells
Current density (mA/cm2)
Voltage (V)
0
5
10
15
20
25
0
0.2
0.4
0.6
0.8
1.0
1.2

Supporting Information

$FAPbI_3$ Perovskite Films Prepared by Solvent Self-volatilization for Photovoltaic Applications

*Qiqi Zhang[a], Guorong Ma[b], Kevin A. Green[b], Kristine Gollinger[a], Jaiden Moore[a], Teresa Demeritte[a], Paresh Chandra Ray[a], Glake Alton Hill Jr[a], Xiaodan Gu[b], Sarah E. Morgan[b], Manliang Feng[c], Santanu Banerjee[c] and Qilin Dai[a]**

[a] Department of Chemistry, Physics, and Atmospheric Sciences, Jackson State University, Jackson, MS, 39217, United States

[b] School of Polymer Science and Engineering, Center for Optoelectronic Materials and Devices, The University of Southern Mississippi, Hattiesburg, MS 39406, United States

c Department of Chemistry and Physics, Tougaloo College, Jacskon, MS, 39174, United States

**Corresponding author: qilin.dai@jsums.edu*

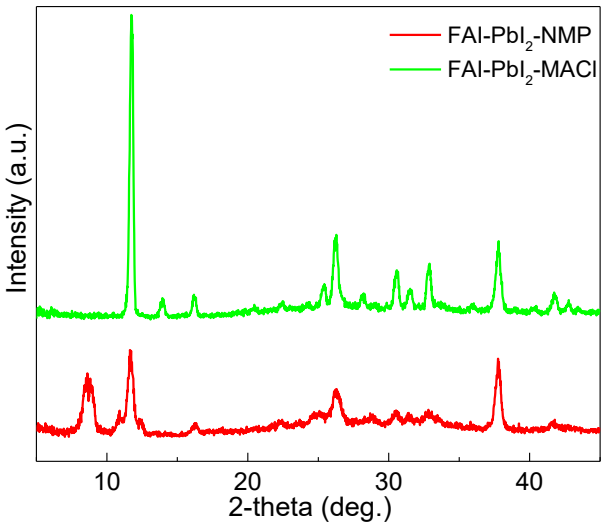

Figure S1. XRD patterns of FAI-PbI_2-NMP and FAI-PbI_2-MACl spin-coated films.

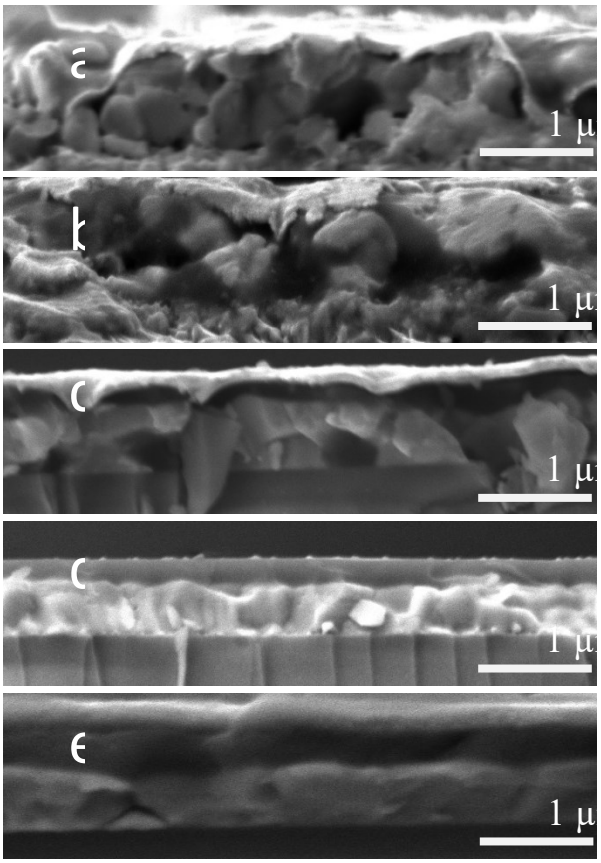

Figure S2. Cross-section for different amount NMP prepared perovskite solar cells. (a). 0% NMP; (b). 2.5% NMP; (c). 5% NMP; (d). 7.5% NMP; (e). 10% NMP.

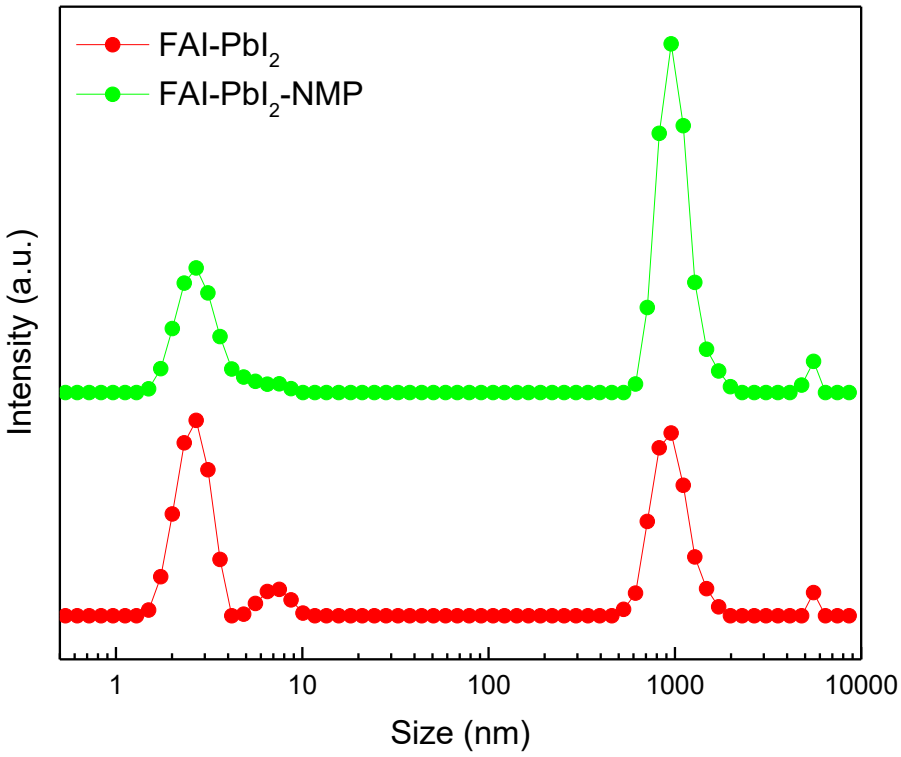

Figure S3. DLS profiles of precursor solutions of FAI-PbI_2 and FAI-PbI_2-NMP in 2-ME.

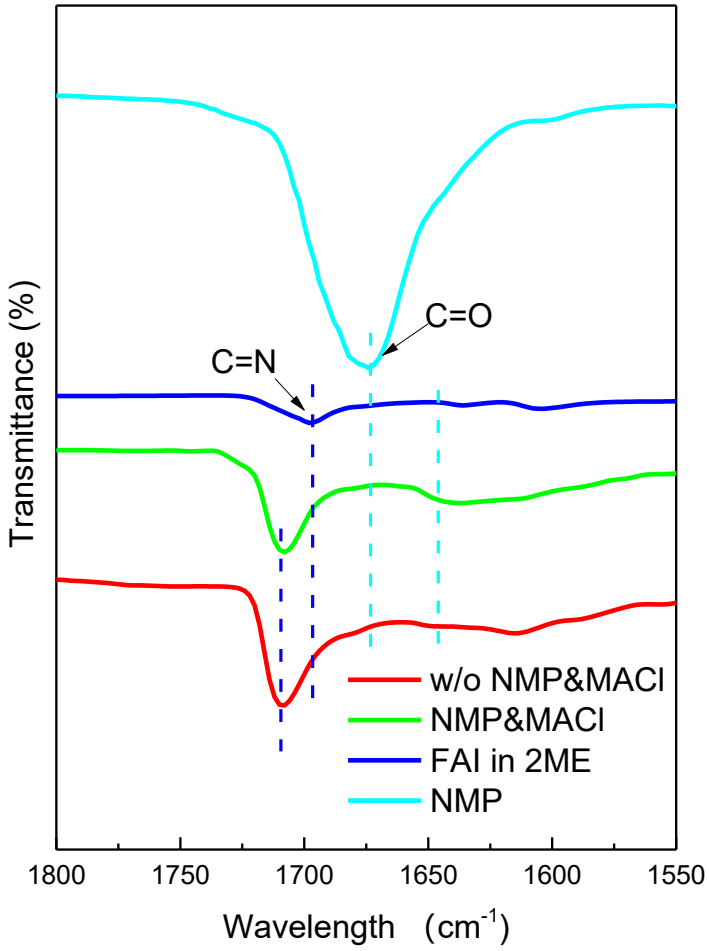

Figure S4. FTIR spectra for FAI and in 2-ME; NMP solvent; perovskite solution without NMP and MACl and perovskite solution with 7.5% NMP and MACl.

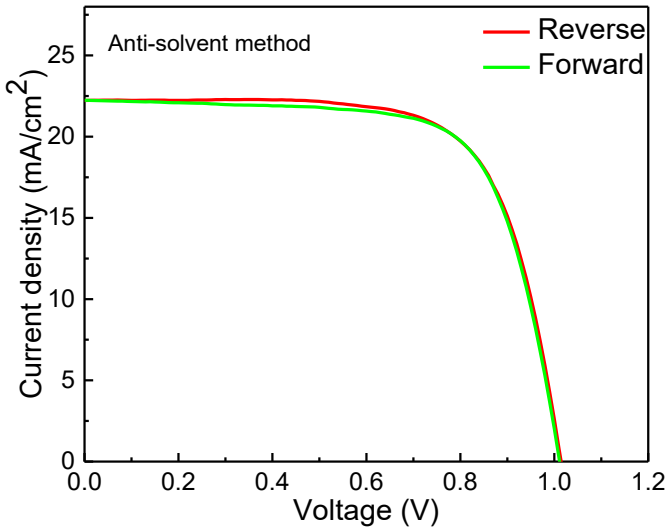

Figure S5. The J-V curves of PSC prepared by antisolvent method measured with the reverse and forward scan directions.

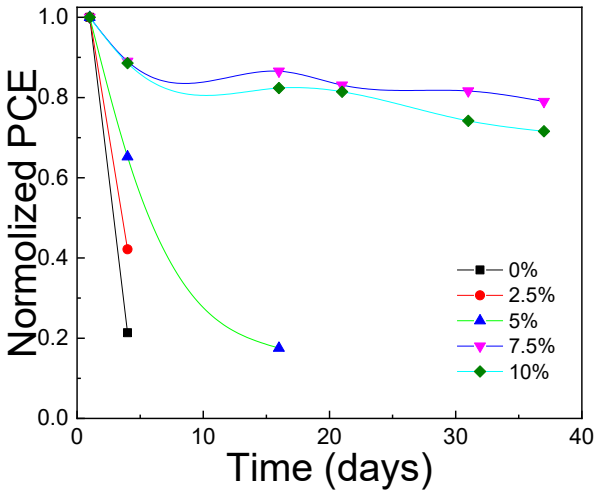

Figure S6. The device aging stability for different amount NMP perovskite solar cell.

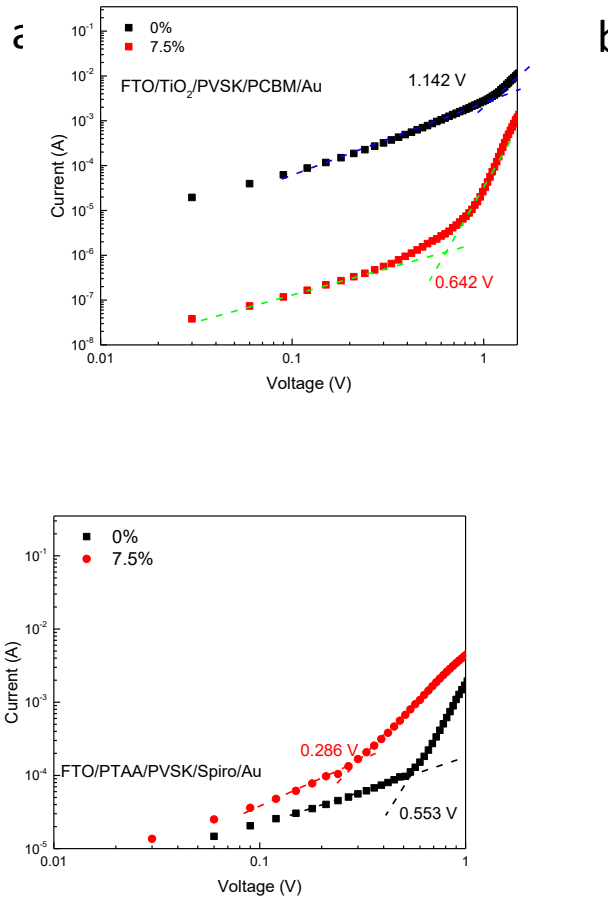

Figure S7. Current-voltage curves of electron-only (a) and hole-only (b) devices based on 0% and 7.5% NMP perovskites.

Table S1. The EIS fitting parameters of different amount NMP devices derived from Fig. 4c.

Sample	**R_s (Ω)**	**R_{rec}(Ω)**	**CPE1 (F)**	**R_{dr}(Ω)**	**CPE2 (F)**
0% NMP	30.13	998	$1.262*10^{-8}$	697.1	$7.034*10^{-7}$
5% NMP	17.28	1842	$1.133*10^{-8}$	5759	$5.898*10^{-9}$
7.5% NMP	17.15	2511	$9.813*10^{-9}$	13120	$2.684*10^{-10}$
10% NMP	19.23	1959	$9.967*10^{-9}$	9860	$2.459*10^{-7}$